Available online at www.sciencedirect.com
SCIENCE DIRECT®
Journal of Magnetic Resonance 172 (2005) 306–311
JMR Journal of Magnetic Resonance
www.elsevier.com/locate/jmr

Relaxation-selective magnetization preparation based on T_1 and T_2

Mark D. Does*

Department of Biomedical Engineering, Radiology and Radiological Sciences, Institute of Imaging Science, Vanderbilt University, USA

Received 16 August 2004; revised 1 November 2004
Available online 7 December 2004

Abstract

A magnetization-preparation scheme is described that combines the spin-echo and inversion-recovery (SEIR) to select spins based on both T_1 and T_2 characteristics. The inclusion of T_2 weighting allows for greater relative suppression of some tissues with respect to others, depending on their respective relaxation times, than does inversion-recovery alone. Formulae describing the observed magnetization following SEIR and double-SEIR (DSEIR) are presented with the corresponding formulae for inversion-recovery (IR) and double-IR (DIR). The formulae are validated with experimental studies on $MnCl_2$ solutions and compared numerically for a variety of possible applications. Results indicate that DSEIR may yield 2× or more signal than DIR in some potential applications.

Keywords: MRI; Inversion-recovery; Double inversion-recovery; Selective excitation; Suppression

1. Introduction

Various pulse sequences exist to selectively prepare magnetization as a function of either T_1 or T_2 relaxation times. Methods based on T_1 have been derived from inversion-recovery (IR) preparations with an appropriate IR delay (t_i) such that spins with a particular T_1 value are saturated. A natural extension of IR for filtering signal of more than one T_1 value is multiple inversion recovery (MIR). With MIR, for every N IR periods, a solution of N t_is exists that will eliminate longitudinal magnetization of spins with N different T_1 times. This method was originally proposed for suppressing background signal in angiograms [1] and has since been used in a variety of applications, including selectively imaging grey or white matter in brain [2,3] and lung parenchyma [4,5]. The drawback of MIR is the concomitant loss of desired signal. For example, Mai et al. [4] quote an 85% reduction of signal from lung parenchyma when double-IR (DIR) was used to suppress signal from surrounding muscle and fat. Similarly, if DIR were used to image only myelin-associated water from nerve or white matter, as suggested recently [6], the myelin–water signal would be reduced by approximately 90%. While Mai et al. still found an increase in contrast-to-noise using DIR, there is no doubt that reducing the suppression of desired signal would significantly increase the efficacy and utility of MIR. In some cases, this may be possible by combining the periods of T_2-weighting in the MIR pulse sequence. Brittain et al. [7] combined spin-echo periods with an inversion-recovery period to create a flow-independent angiography sequence. Similarly, Wong et al. [8] used the combination of spin-echo and inversion-recovery to allow for shorter repetition time (TR) periods in CSF-attenuated imaging of the brain. Herein, the incorporation of spin-echo periods into one or more inversion-recovery periods is considered in general as a means of selective signal suppression based on T_1 and T_2 values.

2. Theory

Consider the simplest scenario, where it is desired to observe one tissue or spin-pool in the absence of another another. Define two spin pools, a and b, assign them

* Fax: +1 615 322 0734.
E-mail address: mark.does@vanderbilt.edu.

1090-7807/$ - see front matter © 2004 Elsevier Inc. All rights reserved.
doi:10.1016/j.jmr.2004.11.008

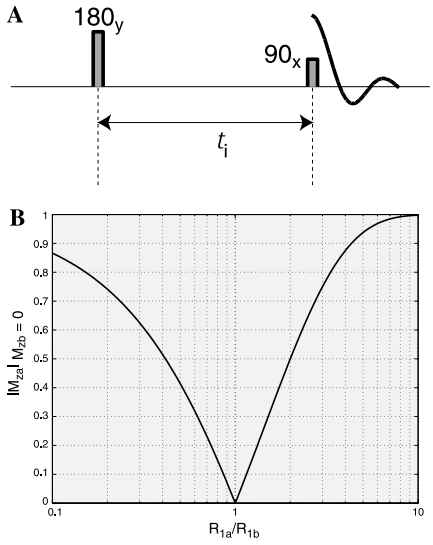

Fig. 1. (A) Diagram of an inversion-recovery pulse sequence and (B) the magnitude of the observed magnetization of spin-pool a when the inversion-recovery sequence is used to null magnetization from pool b, plotted versus the ratio of longitudinal relaxation rates from pools a and b.

relaxation rates, R_1^a, R_2^a, and R_1^b, R_2^b, respectively, and assume an infinite repetition time between acquisitions (for finite TR, see Footnotes 1 and 2). To null longitudinal magnetization from pool b, M_z^b, a simple IR preparation, with inversion time $t_i = \log(2)/R_1^b$ can be used (Fig. 1A). (NB, log refers to the natural logarithm.) The effect of the IR preparation on M_z^a is then easily found to be

$$M^a_{z,\mathrm{IR}}|_{M_z^b=0} = M_0^a(1 - 2\exp(-\log(2)R_1^a/R_1^b)) = M_0^a(1 - 2\cdot 2^{-R_1^a/R_1^b}). \quad (1)$$

Fig. 1B shows the magnitude of M_z^a as a function of the ratio R_1^a/R_1^b and it is clear that IR-preparation works best when this ratio is significantly greater or lesser than unity. Now consider the preparation sequence shown in Fig. 2A, in which a spin-echo (SE) period precedes the IR period (which is thus named the SEIR sequence). In this sequence, the T_2-weighting that results from the spin-echo period results in a different initial condition for the period of longitudinal recovery. Thus, the longitudinal magnetization as a function of the t_e and t_i is[1]

$$M_z(t_e, t_i) = M_0[1 - (1 + \exp(-t_eR_2))\exp(-t_iR_1)]. \quad (2)$$

In this way, a combination of T_2 and T_1 weighting can be used to prepare magnetization from one pool in the absence of the other. To null M_z^b with SEIR, the timings must be

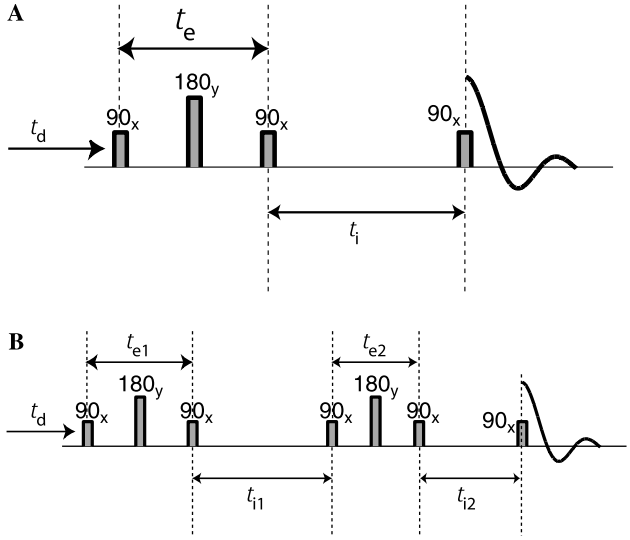

Fig. 2. Diagrams of the (A) spin-echo inversion-recovery and (B) double spin-echo inversion-recovery pulse sequences.

$$t_i = \log[1 + E_e^b]/R_1^b, \quad (3)$$

where

$$E_e^b = \exp(-t_eR_2^b).$$

The effect of this on M_z^a is then

$$M^a_{z,\mathrm{SEIR}}|_{M_z^b=0} = M_0^a\left(1 - (1 + E_e^a)\cdot(1 + E_e^b)^{-R_1^a/R_1^b}\right), \quad (4)$$

where E_e^a is defined similarly to E_e^b in Eq. (3). When the ratio of longitudinal relaxation rates is near unity, $M^a_{z,\mathrm{SIER}}|_{M_z^b=0}$ is approximately equal to $1 - (1 + E_2^a)/(1 + E_2^b)$. Therefore, at the appropriate t_e value, M_z^a approaches $+0.5$ when $R_2^a/R_2^b \gg 1$ and -1.0 when $R_2^a/R_2^b \ll 1$. For a given R_1^a/R_1^b ratio and particular R_2^a and R_2^b values, the t_e value and corresponding t_i that returns the greatest M_z^a magnitude while returning $M_z^b = 0$ can be determined numerically.

To null multiple R_1 components, the extension of SEIR to double or, in general, multiple SEIR periods is straightforward, much like the extension from IR to MIR. Similar to MIR, with more than one SEIR periods, it is not possible to define closed-form solution for pulse sequence timings necessary to null multiple spin pools. Consider a double SEIR (DSEIR) pulse sequence shown in Fig. 2B: the spin-echo periods, t_{e1} and t_{e2}, will modulate the initial conditions of the longitudinal recovery periods, t_{i1} and t_{i2}. The longitudinal magnetization of a given spin pool resulting from this pulse sequence is[2]

[1] If the delay prior to the first 90° pulse (t_d) in Fig. 2A is not many times longer than T_1, then Eq. (2) becomes $M_z(t_e,t_i) = M_0[1 - ([1 - \exp(-t_dR_1)]\exp(-t_eR_2) + 1)\exp(-t_iR_1)]$.

[2] If the delay prior to the first 90° pulse (t_d) in Fig. 2B is not many times longer than T_1, then Eq. (5) becomes $M_z(t_{e1}, t_{e2}, t_{i1}, t_{i2}) = M_0(1 - E_{i2} - E_{i2}E_{e2} + E_{i2}E_{e2}E_{i1} + E_{i2}E_{e2}E_{i1}[1 - E_d]E_{e1})$, where $E_d = \exp(-t_dR_1)$.

$$M_z(t_{e1}, t_{e2}, t_{i1}, t_{i2}) = M_0(1 - E_{i2} - E_{i2}E_{e2} + E_{i2}E_{e2}E_{i1} + E_{i2}E_{e2}E_{i1}E_{e2}), \quad (5)$$

where $E_{ej} = \exp(-t_{ej}R_2)$ and $E_{ik} = \exp(-t_{ik}R_2)$. Note that if $t_{e1} = t_{e2} = 0$, this reduces to the known formula for a DIR sequence

$$M_z(t_{i1}, t_{i2}) = M_0(1 - 2E_{i2} + 2E_{i2}E_{i1}). \quad (6)$$

For a given set of three R_1 and R_2 values, the parameters $\{t_{e1}, t_{e2}, t_{i1}, t_{i2}\}$ in Eq. (5) can be optimized numerically to maximize M_z from one component subject to the constraint that M_z from each of the other two components is less than some prescribed amount. Note that although there are four free parameters, it is not generally possible to saturate M_z of any four R_1 components (excepting the trivial solution where $t_{e2} \gg T_2$ is sufficiently long and $t_{i2} = 0$). Like MIR, the number of components that can, in general, be saturated is equal to the number of IR periods, not the total number of free parameters in the preparation.

3. Methods

3.1. Experimental

To validate the formulae presented above, DIR- and DSEIR-prepared MRI experiments were performed on a phantom of three water-filled tubes, each doped with a different concentration of $MnCl_2$. R_1 and R_2 estimates for each solution were known from previous studies and are shown in Table 1. These relaxation rates were used to determine optimal timings for DIR and DSEIR for the selective excitation of each of the three solutions in the absence of the other two, which are also shown in Table 1. (Note that bathing solution, surrounding the three tubes—see Fig. 3—was not considered in the experiment.) For DIR, t_{i1} and t_{i2} values that result in zero net magnetization from two of the solutions were determined by numerical iteration. For the DSEIR, optimization is more numerically challenging because an infinite number of timing combinations exist to null any two solutions. Thus, timings were optimized to maximize signal from the desired solution, while allowing no more than 0.1% residual signal from either of the other two solutions.

All phantom imaging was done using a standard single-shot, spin-echo EPI pulse sequence, a 35 ms TE, 5 s TR, 50–60 mm FOV, and a 200 kHz BW. To avoid slice profile effects for inversion and refocusing, the slice thickness for the RF pulses was set to twice that of the excitation pulse. Crusher gradients were inserted following inversions and surrounding refocusing pulses to spoil signals from unwanted coherence pathways.

3.2. Numerical

To explore some of the broader utility of incorporating T_2-weighting into MIR preparation sequences, a series of numerical studies was performed. For SIR and SEIR, magnitudes of $M_z^a|_{M_z^b=0}$ depend only on the ratios of relaxation rates involved. Thus, for ranges of R_1^a/R_1^b and R_2^a/R_2^b between 0.1 and 10, $M_{z,\mathrm{IR}}^a|_{M_z^b=0}$ and $\max\{M_{z,\mathrm{SIER}}^a|_{M_z^b=0}, t_e\}$ were calculated and their magnitudes were compared. For DIR and DSEIR, no such global description of their relative performance is possible, so four case scenarios were considered: (1) imaging myelin water in the absence of intra- and extra-axonal water; (2) imaging parenchymal lung water in absence of muscle or fat; (3) distinguishing macromolecular baseline signal (MM) from metabolites of interest (MI) in proton spectroscopy; and (4) imaging white or gray matter in the absence of the other and CSF. For each of these cases, each unique spin pool was assigned longitudinal and transverse relaxation rates estimated from literature [9,10,4,11,6,12], shown in Table 2. Optimal values of $\{t_{i1}, t_{i2}\}$ and $\{t_{e1}, t_{e2}, t_{i1}, t_{i2}\}$ were determined for DIR and DSEIR preparations, respectively, and the resulting signal fraction of the observed pool was determined.

Table 1
Relaxation rates, pulse sequence timings, and experimental observations relating to the MRI measurements of the 3-solution phantom

	R_1 (s^{-1})	R_2 (s^{-1})	DIR timings (ms)		Residual magnetization		DSEIR timings (ms)				Residual magnetization	
			t_{i1} (ms)	t_{i2} (ms)	Predicted M_z/M_0	Observed M_z/M_0 (mean ± SD)	t_{e1} (ms)	t_{e2} (ms)	t_{i1} (ms)	t_{i2} (ms)	Predicted M_z/M_0	Observed M_z/M_0 (mean ± SD)
Solution #1	3.66 (± 0.19)	59.9 (± 1.7)	874	246	0.221	0.228 ± 0.006	46.6	23.7	640	166	0.337	0.354 ± 0.006
Solution #2	2.13 (± 0.03)	16.6 (± 0.5)	718	169	0.093	0.092 ± 0.001	49.6	23.7	417	46.7	0.155	0.157 ± 0.001
Solution #3	1.40 (± 0.03)	9.06 (± 0.6)	546	150	0.134	0.133 ± 0.001	53.1	23.6	215	32.9	0.198	0.200 ± 0.001

For each solution is shown its longitudinal and transverse relaxation rates, the DIR and DSEIR pulse sequence timings necessary to selectively excite that solution in the absence of the other two, and the predicted and observed signal magnitudes normalized to the magnitude of the unprepared, spin-echo signal.

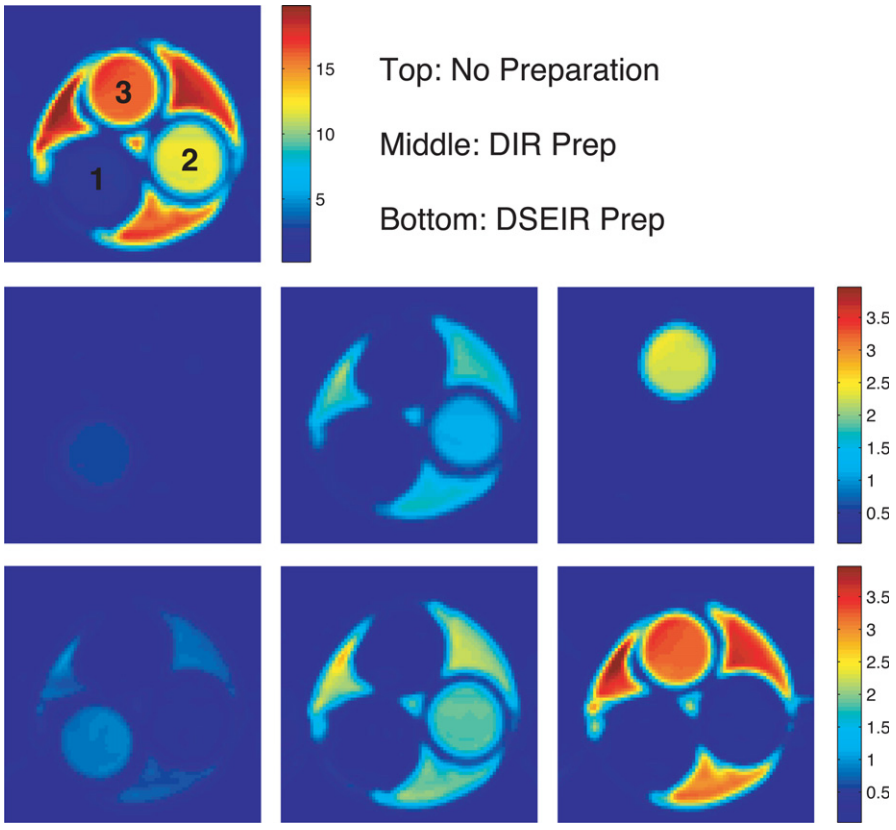

Fig. 3. The top image shows the spin-echo signal intensity for all three $MnCl_2$ solutions (labelled #1, #2, and #3, in correspondence to Table 1). Note that the contrast between solutions in this frame results from the T_2-weighting of the spin-echo alone, as no magnetization preparation was employed and the TR was relatively long. The rows of images in the middle and bottom of the frame show the same solutions following DIR and DSEIR preparations, respectively. Preparations were designed to eliminate signal from solutions #2 and #3 in the leftmost images, #1 and #3 in the central images, and #1 and #2 in the rightmost images. In all cases signal elimination was successful, but all DSEIR-prepared images show higher signal magnitude from the remaining solution (as demonstrated numerically in Table 1).

Table 2
Observed magnetization magnitudes between DIR and DSEIR preparation pulse sequences for several scenarios

	T_1, T_2 (ms)	Optimal DSEIR timings $\{t_{e1}, t_{i1}, t_{e2}, t_{i2}$ (ms)	M_z (DIR)	M_z (DSEIR)	Increase (%)
Myelin/axon/extra-axon (@ 7 T, excised)	**(876, 17)**, (1540, 60), (2023, 170)	107.2, 1834, 19.3, 592	0.20	0.35	72
Myelin/axon/extra-axon (@ 4.7 T, in vivo)	**(940, 12)**, (1330, 33), (1845, 105)	64.7, 1509, 14.8, 45.2	0.10	0.24	132
Lung/fat/muscle (@1.5 T)	**(1300, 90)**, (250, 60), (930, 30)	82.8, 56.1, 0, 0	0.16	0.34	115
MI/MM/MM (@1.5 T)	**(1000, 300)**, (250, 40), (150,15)	59.4, 77.4, 19.6, 15.1	0.53	0.65	22
WM/**GM**/CSF (@3.0 T)	(830, 80), **(1330, 110)**, (4500, 2200)	285, 3487, 0, 568	0.23	0.25	10
WM/GM/CSF (@3.0 T)	**(830, 80)**, (1330, 110), (4500, 2200)	284, 3942, 0, 886	0.30	0.32	6

The tissue being selectively excited and whose magnitudes are presented is defined for each row with bold characters. MI, metabolites of interest; MM, macromolecular baseline; WM, white matter; GM, grey matter; and CSF: cerebrospinal fluid.

4. Results and discussion

Experimental validation of the DSEIR pulse sequence is shown in Fig. 3 and Table 1. In Fig. 3, the top image shows the unprepared spin-echo signal intensity for all three $MnCl_2$ solutions (labelled #1, #2, and #3, in correspondence to Table 1). The rows of images in the middle and bottom of the frame show the same solutions following DIR and DSEIR preparations, respectively. Preparations were designed to selectively excite signal from solution #1 in the leftmost images, #2 in the central images, and #3 in the rightmost images, using pulse sequence timings listed in Table 1. The predicted and observed values of normalized signal magnitude from the selected solutions corresponded quite closely: observed values of solutions 2

and 3 deviated from the predicted values by less than 0.25% (of unprepared signal), while the observed value for solution #1 was ≈2% above the predicted value. Similar results were found for the nulled signals (not shown): solutions #2 and #3 were reduced to ⩽0.8% of their unprepared magnitudes in all cases, while solution #1 was reduced to 2.1 and 1.1% when selecting for solutions #2 and #3, respectively. The deviations between predicted and observed values were most likely due to a combination of image noise in the EPI acquisition and an inaccurate T_1 and/or T_2 estimate for solution #1.

A more general evaluation of incorporating SE periods with IR periods for magnetization preparation is shown in Fig. 4 and Table 2. The relative performance of IR vs SEIR can be briefly summarized, because both $M^a_{z,\mathrm{IR}}|_{M^b_z=0}$ and $\max\{M^a_{z,\mathrm{SIER}}|_{M^b_z=0}, t_e\}$ depend only on the ratio of relaxation rates, R^a_1/R^b_1 and R^a_2/R^b_2. Fig. 4A shows the magnitude of $M^a_{z,\mathrm{SIER}}|_{M^b_z=0}$ with optimized t_e and as a function of R^a_1/R^b_1 and R^a_2/R^b_2. Although optimal t_e values change with absolute values of R^a_2 and R^b_2, the magnitude of M^a_z depends only on their ratio (and the ratio of R_1s). In Fig. 4B is the difference between the magnitudes of $M^a_{z,\mathrm{IR}}|_{M^b_z=0}$ and $\max\{M^a_{z,\mathrm{SIER}}|_{M^b_z=0}, t_e\}$. In regions where this image shows zero difference, the optimal t_e value for SEIR is zero, thereby reducing it to a simple IR preparation. As apparent from the figure, SEIR is generally advantageous when R^a_1/R^b_1 is near unity and R^a_2/R^b_2 is not, which makes sense because IR alone performs well when R^a_1/R^b_1 is far from unity (Fig. 1B). More specifically, SEIR offers greatest potential when spins with relatively large R_2 values are being nulled (left side of Figs. 4A and B), but may be advantageous in the converse circumstance as well.

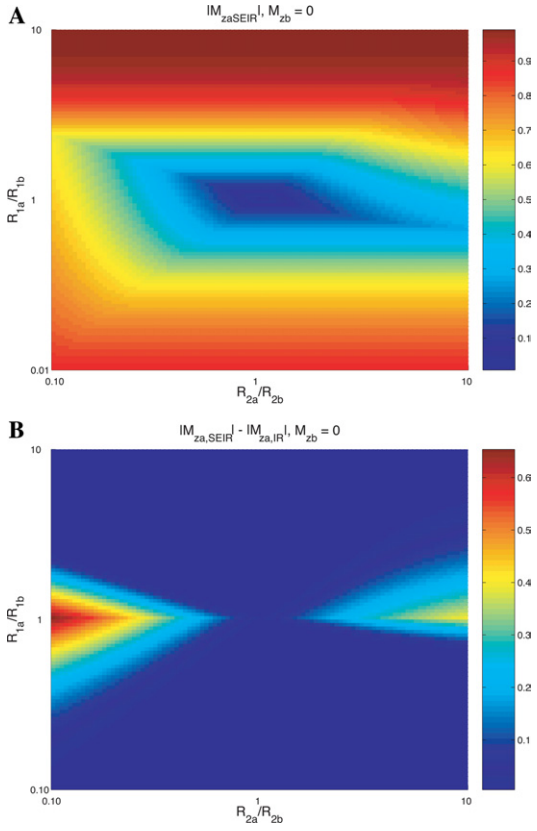

Fig. 4. Images describing the performance of the SEIR pulse sequence. In (A) is shown magnitude of the observed magnetization of spin-pool a when the SEIR sequence is used to null magnetization from pool b and t_e has been chosen maximize signal from pool a. Data are presented as a function of the ratios of longitudinal and transverse relaxation rates between pools a and b. In (B) is shown the difference between the data in (A) and the magnitude of the observed magnetization of spin-pool a when the IR sequence is used to null magnetization from pool b (as shown in Fig. 1B). That is, frame (B) shows the domain of R^a_1/R^b_1 and R^a_2/R^b_2, where SEIR offers an advantage over IR.

For DIR (or MIR, in general) it is not possible to create one image that demonstrates the relative effectiveness of including SE periods into the pulse sequence. Consequently, the efficacy of DIR is shown in Table 2 for several case scenarios. Table 2 shows the fraction of signal measured using DIR and DSEIR in five example tissue combinations. In each case, the tissue or tissue compartment in bold is the component being measured, while the other two components are eliminated or reduced to <0.1% equilibrium amplitude for the DIR and DSEIR preparations, respectively. Also shown are the optimal pulse sequence timings for the DSEIR preparations. In Fig. 5 are images to accompany three of the scenarios in Table 2, which show the response of M_z as a function of T_1 and T_2.

Not surprisingly, the extent to which DSEIR can increase signal is dependent on the specific relaxation times involved. Substantial increases are seen in myelin water and parenchymal lung water for DSEIR compared to DIR. Using DSEIR to distinguish some metabolites of interest (with $T_1/T_2 = 1000/300$ ms) from a macromolecular baseline offers a modest advantage (22%), and for distinguishing white or grey matter from the each other and cerebrospinal fluid, DSEIR yields less than a 10% signal increase.

It is worth noting that all four phases of the magnetization preparations are not always necessary. Selecting parenchymal lung water while suppressing surrounding fat and muscle can be achieved optimally with only a single SEIR preparation, as apparent from the zero values of t_{e2} and t_{i2} in Table 2. In the lower middle image in Fig. 5, it can be seen that both fat and muscle lie along a single locus of suppressed signal in T_1–T_2 space. It is also apparent from Fig. 5 that the sensitivity of DSEIR preparation to relaxation time estimates is similar to that of DIR, but depends on both T_1 and T_2 estimates, rather than just T_1. Thus, in some cases, DSEIR may be relatively insensitive to the estimated T_1 value of suppressed components, but more sensitive to their T_2 estimates.

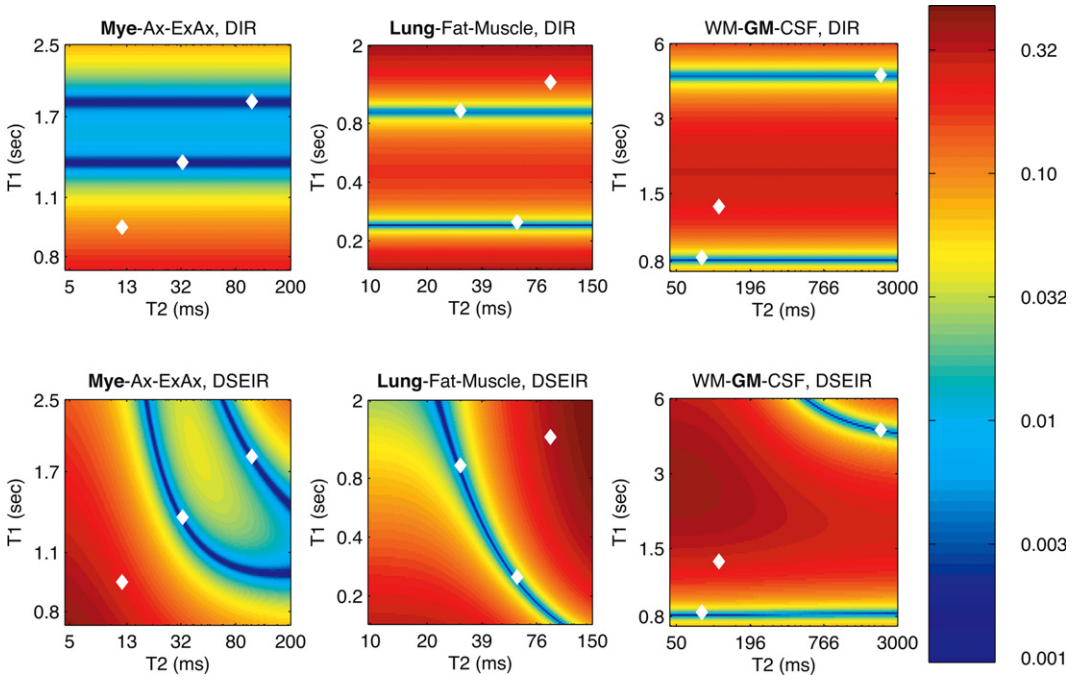

Fig. 5. Performance of DIR and DSEIR magnetization preparation for three of the example scenarios shown in Table 2. Each image displays the magnitude of M_z on a log scale as a function of both T_1 and T_2. As expected, the DIR preparations demonstrate sensitivity only to T_1, while the DSEIR preparations reveal a complex sensitivity to T_1 and T_2. Diamonds indicate the T_1–T_2 values of each tissue component, as listed in Table 2.

5. Conclusion

Combining periods of spin-echo weighting with inversion-recovery periods can significantly increase the observed signal magnitude compared to inversion-recovery preparation alone. This increased signal may be of particular value when multiple inversion recovery periods are used to null multiple specific T_1 components or a broad range of T_1 values, although a determination of efficacy must be performed numerically for each unique situation. Also, unlike using inversion-recovery alone, spin-echo inversion-recovery preparations require a priori estimates of both T_1 and T_2 values for each spin pool, although the necessary accuracy of these estimates will vary for each unique situation.

Acknowledgments

These studies were supported by funding from NIH/NIBIB, #R01-EB001744.

References

[1] W.T. Dixon, M. Sardashti, M. Castillo, G.P. Stomp, Multiple inversion recovery reduces static tissue signal in angiograms, Magn. Reson. Med. 18 (2) (1991) 257–268.
[2] T.W. Redpath, F.W. Smith, Use of a double inversion-recovery pulse sequence to image selectively grey or white brain matter, Br. J. Radiol. 67 (804) (1994) 1258–1263.
[3] P.A. Boulby, M.R. Symms, G.J. Barker, Optimized interleaved whole-brain 3D double inversion recovery (DIR) sequence for imaging the neocortex, Magn. Reson. Med. 51 (6) (2004) 1181–1186.
[4] V.M. Mai, J. Knight-Scott, S.S. Berr, Improved visualization of the human lung in 1H MRI using multiple inversion recovery for simultaneous suppression of signal contributions from fat and muscle, Magn. Reson. Med. 41 (5) (1999) 866–870.
[5] V.M. Mai, Q. Chen, A.A. Bankier, R.R. Edelman, Multiple inversion recovery MR subtraction imaging of human ventilation from inhalation of room air and pure oxygen, Magn. Reson. Med. 43 (6) (2000) 913–916.
[6] M.D. Does, J.C. Gore, Compartmental study of T(1) and T(2) in rat brain and trigeminal nerve in vivo, Magn. Reson. Med. 47 (2) (2002) 274–283.
[7] J.H. Brittain, E.W. Olcott, A. Szuba, G.E. Gold, G.A. Wright, P. Irarrazaval, D.G. Nishimura, Three-dimensional flow-independent peripheral angiography, Magn. Reson. Med. 38 (3) (1997) 343–354.
[8] E.C. Wong, T.T. Liu, W.M. Luh, L.R. Frank, R.B. Buxton, T(1) and T(2) selective method for improved SNR in CSF-attenuated imaging: T(2)-FLAIR, Magn. Reson. Med. 45 (3) (2001) 529–532.
[9] K.L. Behar, D.L. Rothman, D.D. Spencer, O.A. Petroff, Analysis of macromolecule resonances in 1H NMR spectra of human brain, Magn. Reson. Med. 32 (3) (1994) 294–302.
[10] J. Knight-Scott, Application of multiple inversion recovery for suppression of macromolecule resonances in short echo time (1)H NMR spectroscopy of human brain, J. Magn. Reson. 140 (1) (1999) 228–234.
[11] J.P. Wansapura, S.K. Holland, R.S. Dunn, W.S. Ball Jr., NMR relaxation times in the human brain at 3.0 tesla, J. Magn. Reson. Imaging 9 (4) (1999) 531–538.
[12] A.R. Travis, M.D. Does, Myelin selective magnetization preparation, in: Proceedings of the Society of Magnetic Resonance in Medicine, Twelfth Scientific Meeting (Kyoto), 2004, p. 178.